Available online at www.sciencedirect.com
ScienceDirect
ELSEVIER
Journal of Solid State Chemistry 179 (2006) 4056–4065
JOURNAL OF SOLID STATE CHEMISTRY
www.elsevier.com/locate/jssc

Rapid communication

Evaluation of the initial growth of electroless deposited Co(W,P) diffusion barrier thin film for Cu metallization

Aaron Zhu[a,*], Yossi Shacham-Diamand[b,c], Mark Teo[a]

[a] *Advanced Materials and Engineering Processing Laboratory (AMPEL), University of British Columbia, 2355 East Mall, Vancouver, British Columbia, Canada V6 T 1Z4*
[b] *School of EE, Tel-Aviv University, Ramat-Aviv, 69978, Israel*
[c] *School of Applied Chemistry, Waseda University, Shijuku-ku, Toyko 169-8555, Japan*

Received 24 June 2006; received in revised form 30 August 2006; accepted 1 September 2006
Available online 16 September 2006

Abstract

The formation mechanism of electroless deposited Co(W,P) films is investigated. Co(W,P) films, containing 88–90 at% of Co and 10–12 at% of W and P, are deposited directly onto p-type Si(100) substrate via Pd wet activation. Co(W,P) initially nucleates around Pd activation sites and this is followed by a strong lateral growth. Uniform Co(W,P) thin films can be obtained after 2 min deposition. Fast immersion measurement shows that the mixed potential of Co(W,P) is −0.78 V versus Ag/AgCl electrode. XRD examination shows that the Pd layer has a domination of (111) texture and the principle microstructure of the as-deposited Co(W,P) film is the hcp phase of nano-sized ε-Co. The inelastic mean free path of diffused Cu in Co(W,P) is determined to be 7.37 Å which is significantly smaller than that (9.9 Å) in pure Co, indicating that Co(W,P) is a very effective barrier layer.
© 2006 Elsevier Inc. All rights reserved.

Keywords: Scanning tunneling microscopy (STM); Thin films; Co(W,P); Deposition; Crystal growth

1. Introduction

Complete Cu metallization is regarded to be the next generation of ultra-large-scale-integration (ULSI) and micro-electro-mechanical system (MEMS) since it offers significant improvements in both performance and reliability compared to the presently used Al and Al–Cu metallization. However, difficulties of implementing Cu metallization include the drift of Cu ions into the inter-level dielectrics (ILDs), the fast diffusion of Cu in Si as well as the creation of electrically active deep level in the energy band gap [1]. Therefore, developing a new diffusion barrier layer between Cu and Si or a new ILD is technologically important [2–5].

Although TaN is currently established as the best material for use in the barrier layer, it suffers from several drawbacks. First, the conductivity of TaN based materials is relatively low (ca. 2700 μΩ cm of resistivity) and with the line-width narrowing in the integrated unit, a barrier layer material with higher conductivity is required. Secondly, TaN is comprised of several equilibrium phases and metastable structures [6,7], hence changing the N/Ta atomic ratio can consequently alter the film structure and its properties. Furthermore, TaN-based films can only be deposited by physical vapor deposition (PVD) and chemical vapor deposition (CVD) methods which cannot produce the conformality in via and trench. Atomic level-deposition (ALD) is the latest method developed for TaN deposition but it is still in its infancy. Electroless deposition is the currently favored technique for semiconductor manufacturing not only because it is simple and economical, but also because it provides the conformal uniformity of deposition in via and trench as well as the controllable film thickness (<10 nm) as required in industry. However, this method cannot yet be applied for preparing TaN-based materials because of the difficulty of finding a suitable deposition solution recipe.

Co(P) was examined as an effective barrier against Cu diffusion up to 400 °C [8,9]. The presence of an amorphous

*Corresponding author. Fax: +1 604 822 47450.
E-mail address: researchman12001@yahoo.com (A. Zhu).

0022-4596/$ - see front matter © 2006 Elsevier Inc. All rights reserved.
doi:10.1016/j.jssc.2006.09.002

phase or Co(P) intermetallics in the microstructures of such material can play a key role in preventing the diffusion of Cu into Si. Nevertheless, its resistivity (ca. 80 μΩ cm) and adhesive features are not satisfactory. The discovery of the barrier properties of thin electroless Co(W,P) films with lower resistivity (ca. 30 μΩ cm) presents new opportunities in Cu passivation and barrier technology [10–12]. Co(W,P) films demonstrate good adhesion to Cu and many other ILD films [3,4,11,12]. Additionally, Co(W,P) can be electroless deposited and has a very good conformal ability in filling the high-aspect-ratio via/trench. Co(W,P) can also be deposited directly onto Si, yielding uniform films with strong adhesion to the substrate and this could be promising for application of making contacts for Si MEMS devices.

Co(W,P) has been recently tested by American and Japanese semiconductor manufacturers (e.g. Sony, Intel, Applied Materials, etc.) and their feedback indicates that the initial deposition control in the formation of Co(W,P) metal coatings have a profound impact on their microstructure as well as their overall functional properties. Properties of Co(W,P) thin films such as adhesion, strength and microstructures are dependent upon the deposited metal nucleus characteristics. In order to improve the performance of Co(W,P) in commercial products, a detailed, nano-scaled investigation on the initial formation stages of Co(W,P) should be pursued.

Scanning tunneling microscopy (STM) and atomic force microscopy (AFM) are extremely powerful analysis tools for atomic-scaled studies. In-situ tracing of electroless deposition of metal via STM/AFM is not available since the spontaneously deposited metal particles would block the end of the tip, making it impossible to realize imaging. However, STM and AFM were successfully utilized for ex-situ observations of the initial formation stage of the electroless deposited metal materials [13–16]. Thus, in this work, the study of nucleation sites and film growth, the changes of grain size influenced by a modified electroless deposition bath, the study of successive nucleation processes of electroless Co(W,P) alloying onto Pd-activated Si wafer surface as well as a fundamental evaluation of Co(W,P) are presented. These studies were conducted via STM in conjunction with high resolution scanning electron microscopy (HRSEM), signal enhancement X-ray diffraction (SEXRD), scanning auger microscopy (SAM) and electrochemical fast immersion microscopy (EFIM).

2. Experimental

2.1. Sample preparation

Analytical reagent grade chemicals (Alfa Products) and double de-ionized water (DDW, Milli-Q, 18.3 MΩ cm) were used for bath preparation. The samples were ca. 1 cm^2 single-crystal Si substrates that were cut from the standard p-type Si(100) wafers (B doped, 1.5×10^{15} cm^{-3}, eWafer International) with 10 Ω cm resistivity. Prior to electroless plating, the substrates were dipped in the standard bath 1 then in bath 2 described in Table 1 for 5 min in each bath for cleaning and degreasing. The degreasing effect was occasionally examined by X-ray photoelectron microscopy (XPS). Next, the samples were treated in a mixture of HF (49 vol%) and NH_4F (40 vol%) in a volume ratio of 1:10 at room temperature (2 min) to improve adhesion. The Si surface then was dipped in Pd activation solution (Table 2) for 2–10 min. Samples were rinsed in DDW after each step. Electroless Co(W,P) plating was conducted at 90–91 °C for periods of 1 s–45 min in the chemical bath (Table 3).

2.2. Electrochemical fast immersion measurement

Co(W,P) electroless depositions on Pd was studied in-situ by measuring the mixed potential of the oxidation/reduction system as a function of time because the establishment of mixed potential is directly related to the thermodynamics and kinetics of the deposition process. The so-called fast immersion (FI) technique, a process where the sample is quickly dipped into the solution with its potential measured, was selected for this investigation.

Table 1
Composition of the solutions for substrate treatment prior to deposition

	Bath I	Bath II
	H_2O_2:HCl:H_2O	H_2O_2:NH_4OH:H_2O
Volume ratio	1:1:5	1:1:6
Temperature (°C)	80	80
Time (min)	5	5

Table 2
Composition of a Pd activation solution in a 1L solution

Component	Concentration
$PdCl_2$	2.2 mM
HCl (36%)	2 ml
Glacial acetic acid	16.7 M
HF (48%)	10 ml

Table 3
Composition of an electroless Co(W,P) deposition solution

Component	Concentration
$CoSO_4 \cdot 7H_2O$	0.082 mol/l
$Na_3C_5H_5O_7 \cdot H_2O$	0.492 mol/l
H_3BO_3	0.502 mol/l
$Na_2WO_4 \cdot 2H_2O$	0.03 mol/l
$NaH_2PO_2 \cdot 2H_2O$	0.169 mol/l
KOH	Adjusted pH to 8.9–9.0
RE-610 (surfactant)	0.05 g/l

Note: $Na_3C_5H_5O_7 \cdot H_2O$ is sodium citrate di-hidrate, RE-610 is the commercial name of a wetting agent made by Roche company (USA).

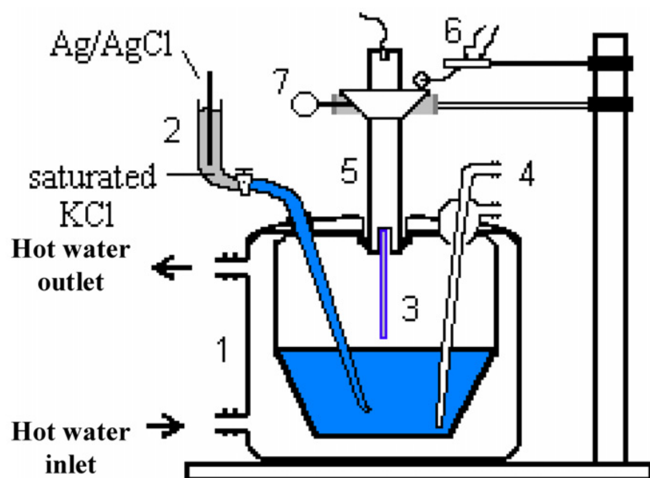

Scheme 1. Set-up of Fast Immersion measurement. Legend: (1) jacketed glass cell; (2) reference electrode compartment; (3) the sample; (4) bubbler for deaeration; (5) sample holder; (6) microswitch for triggering the oscilloscope; (7) pulling out this pin allows the sample to fall into the solution and the measurement starts.

FI chronovoltametry is the unique in-situ approach to synchronously monitor the electroless deposition process and this provides the true thermodynamic and kinetic information of deposition evolution. FI measurements are required to avoid interference between the build-up electrolytic double-layer on the electrode/solution interface and the deposition process. All the potential values mentioned in this paper were referenced to the commercial Ag/AgCl reference electrode (EG&G, USA). To monitor the potential changes of working electrode during deposition, a TDS 430A 12-bit digitizing oscilloscope (Tektronix, USA) was employed. A sampling frequency of 100 samples s^{-1} was used, and 60,000 samples were collected thus leading to a measuring time of 600 s. Experimental setup of FI is shown in Scheme 1.

2.3. Instrumentation

The crystalline structure and orientation of Co, Pd and Co(W,P) films were determined by a signal enhancement powder X-ray diffraction (SEXRD, Sintag) using Cu$K\alpha_1$ radiation on a Sintag diffractometer equipped with the Bragg–Brentano θ–2θ configuration. A NanoScope II (Digital, USA) scanning tunneling microscope (STM) was used to ex-situ monitor the evolution of Co(W,P) film deposition. The final film morphology was examined by both STM and high-resolution scanning electron microscope (HRSEM, Jeol JSM-800 and LEO Gemini 982 with a field emission gun were used respectively). scanning auger microscopy (SAM) and X-ray photoelectron spectroscopy (XPS) in the PHI 590A system were used to detect the initial growing sites of Co(W,P) on Pd wet-activated silicon substrate as well as to measure the inelastic mean free path of diffused Cu in the Co(W,P) barrier layer. Prior to the experiments, all instruments were calibrated using standard methods. A Tencor alpha step profilometer (Tencor, USA) was employed to measure the thickness of sample surface steps that were made by the etching technique developed in our laboratories.

3. Results

3.1. Co(W,P) nucleation and growth on Pd

3.1.1. Observation of nucleation and early stages of deposition

In order to perform an observation somewhat like an in-situ monitoring prior to deposition, a crush mark was made by using AFM in the examined area of Si wafer surface. From scanning auger microscope (SAM) analyses, an electron micrograph of an etched p-type Si(100) surface was identified to have two distinct zones of Si and Pd (Fig. 1a) while an Auger elemental line scan (lateral resolution of 100 nm) across the interface showed its Pd profile distribution (Fig. 1b). The etched Si surface (area left of the interface in Fig. 1a) is rough and irregular and this is confirmed by STM (Fig. 2a). On the other hand, STM showed that the etched Si surface that is activated with Pd (area right of the interface in Fig. 1b) contains shallow deposition rows with grains that are more spherical and more densely packed (Fig. 2b taken from the right border of the interface). Ex-situ high resolution SEM images of Pd activated Si wafer surfaces before and after 1 s

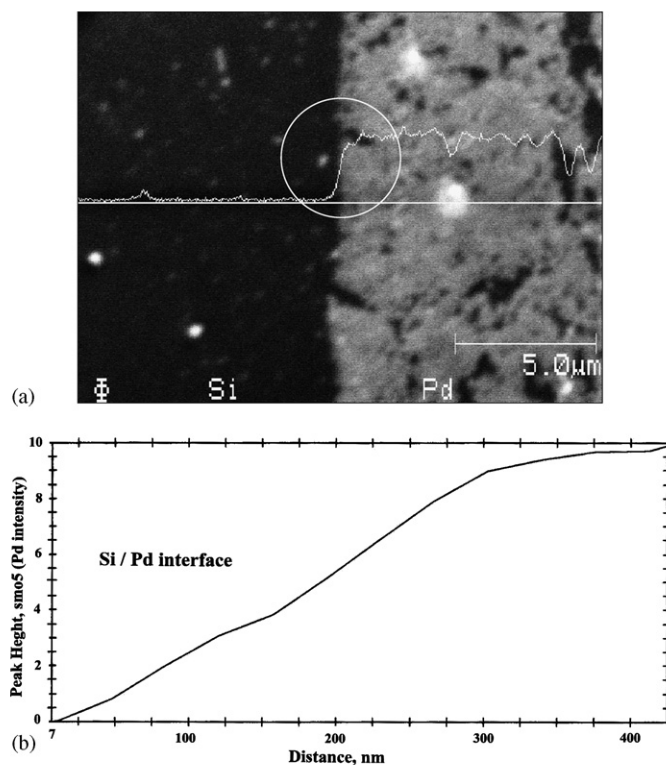

Fig. 1. Auger elemental line scan superimposed on the SEM image as obtained from scanning auger microscopy (SAM) of (a) Pd deposited on etched Si wafer surface and (b) Pd distribution at the Pd/Si lateral interface.

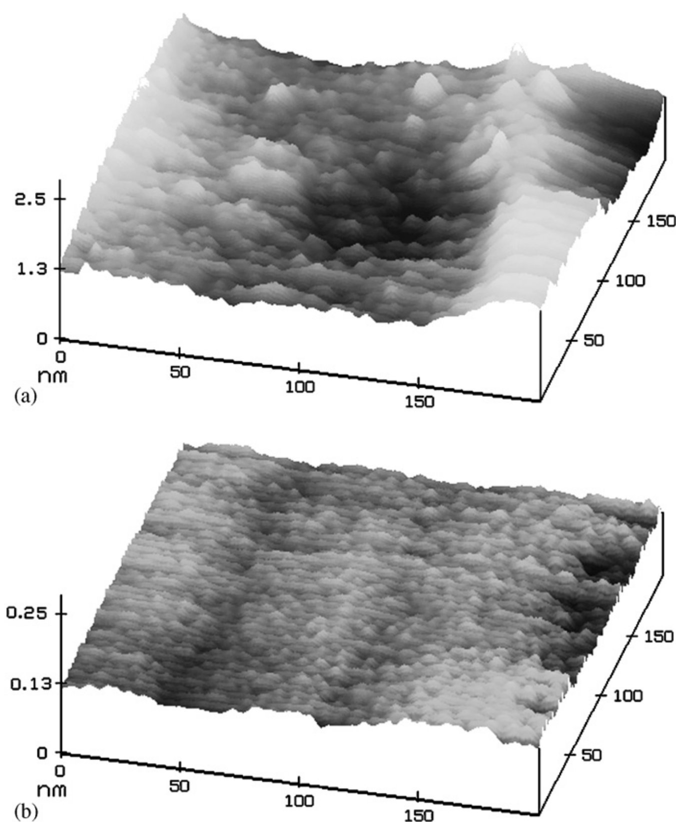

Fig. 2. STM morphologies of (a) etched p-Si(100) surface and (b) Pd activated Si surface. The images were taken from the both sides of the interface of Fig. 1(a). Scanning scale: 200×200 nm.

of Co(W,P) deposition were shown in Figs. 3a and b respectively and, SAM measurement confirms the existence of Co. This clearly indicates that Co(W,P) nucleates at Pd sites but not at the area between the Pd seeds. An STM image (10×10 nm) of the Pd activated Si surface (for distinguishing the different deposit features, the STM detective area was taken in a flat area very close to a "ball" shown in Fig. 3b) after 1 s Co(W,P) deposition is seen in Fig. 4. In order to resolve the deposits, the original images were filtered and reconstructed using a three-step filtering process that was integrated into the software of the NanoScope II STM (Digital Instruments) [17]:

1. The 2D spectrum of the image was calculated by fast Fourier transformation (FFT).
2. Peaks containing periodic structural information were selected by using low-pass filtering twice.
3. The improved original image was calculated using the 2D auto-correlation function.

This resulted in processed 5×5 nm and 2×5 nm images (Figs. 5a and b respectively) from which an arrangement between Pd and Co(W,P) was derived. Areas with atomic spacings of 0.40 ± 0.02 nm and 0.25 ± 0.02 nm were found. From SAM analyses, areas with the atomic spacing of 0.40 ± 0.02 nm primarily have Pd seeds while Co nuclei are conspicuous in the areas with the atomic spacing of 0.25 nm. Two additional STM experiments were performed to the two electroless deposited samples of which one was deposited only Pd while another has solely Co. The analyses to the processed images using the three-step filtering procedure mentioned above suggested that 0.40 nm *d*-spacing is surely dominant in the sample with only Pd whereas 0.25 nm *d*-spacing can only be found in the sample with only Co. Therefore, Co(W,P) nucleation seems to initiate at the periphery of Pd, which means that the reduction of Co^{2+} occurs at the surrounding sites of the previously precipitated Pd clusters. Thus, Co(W,P) electroless deposition is most likely to be electrochemical in nature as it follows the electrochemical reaction mechanism proposed by Hwang et al. and Osaka. et al. [14–16]. No other characteristic atomic spacings were found in the Co(W,P) samples and this indicates that Co first deposits onto the surface in Co(W,P) electroless deposition.

After 2 s of deposition, SEM shows agglomeration of the deposits (Fig. 6a). The corresponding STM morphology depicts some fine fluctuation zones containing 3D deposited particles 2–4 nm in diameter (Fig. 6b). Agglomerated grains in these zones are compact, indicating that continuous nucleation has occurred. The deposition time of 3 s is characterized by the growth evolution similar to that of 2 s as STM showed Co nuclei coalescing in the horizontal direction to form a very thin but still discontinuous metal deposit (Fig. 7). The grain size of the 3 s deposit (0.35–0.9 nm as measured by STM) shows a marked decrease compared with that of the 2 s deposit and

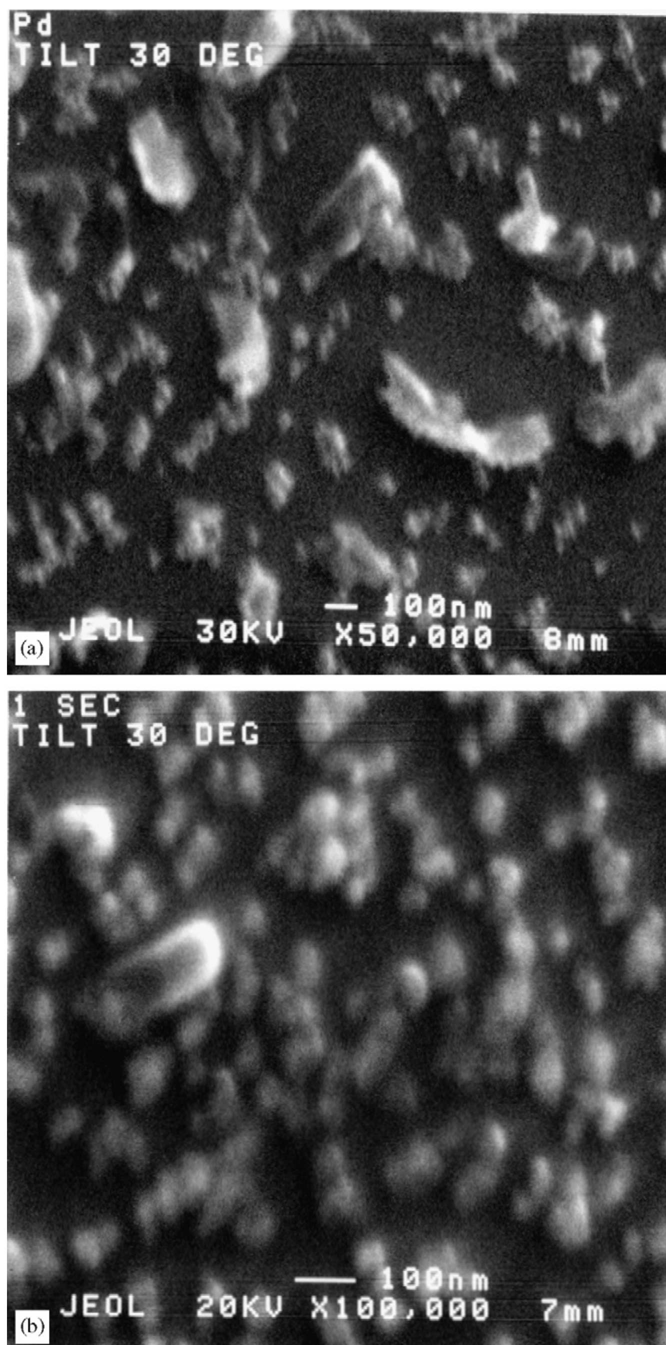

Fig. 3. Quasi in-situ SEM morphologies of the Pd activated Si surface (a) before Co(W,P) deposition and (b) after 1 s Co(W,P) deposition.

this phenomenon implies that continuously fine nuclei are being created.

Fig. 8 represents the Enhancement Signal X-ray spectrum of 10 s deposited Co(W,P). Even though the in-halo Co signal is weak from the thin film, it can be still distinguished from the signal of the Si substrate. From XRD spectral analysis, the in-halo Co signal is consistent with nano-sized Co in the hcp structure. The related STM image (Fig. 9) demonstrates that some new nodule clusters have emerged. SAM element analyses to the area with these nodules indicate that those nodule clusters areas contain about 0.8 at% W and 1–2 at% P.

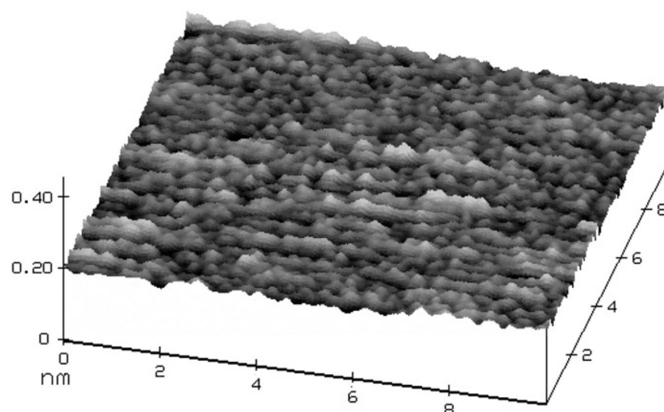

Fig. 4. Original morphology (10×10 nm) of the Pd activated Si surface after 1 s electroless deposition of Co(W,P).

3.1.2. Observation of thin film growth

After 45 s of deposition, the film is ca. 100 nm thick while growing agglomerates completely merge and form a continuous film as observed by STM (Fig. 10). Strong grain growth of varying degrees is observed. Upon further inspection, typical layer-by-layer growth (Frank–van der Merwe growth mode) is revealed since the preceding deposited layer acts as an underlayer for the following one. The newly deposited layer then adopts a relatively flat appearance and spreads layer-by-layer until it covers the whole surface. When grains developing along two different orientations meet each other, a splice is formed. This restrains the grains from propagating along their original directions. Thus, the edges of deposited layer appear in the form as presented in Fig. 10. Further prolongation of deposition time to 10 min leads to the formation of cracks and voids as well as the distorted arrangement of grain rows in the film as observed from Fig. 11. This indicates that the formation process of Co(W,P) coating is accompanied by increasing surface strains and stress.

3.2. Fundamental evaluation of Co(W,P) in MOS structure

3.2.1. Effect of underlayers on kinetics of deposition-fast immersion measurement

The fast immersion (FI) curve on Pd activated Si surface (Fig. 12) illustrates that the mixed potential drops dramatically from 0.0 to -0.37 V within the first 5 s of deposition. This indicates the change in surface energy is caused by electrochemical wetting and Pd activation. The energy barrier was observed to decrease by 0.74 eV (since the potential changes from 0.0 to -0.37 V and two electrons are transferred in the reaction of $Co^{2+} + 2e^- \rightarrow Co^0$). A marked spike was observed in the FI afterwards and this is followed by a short fluctuation plateau characterizing the inhomogeneous Co(W,P) electroless deposition at different sites of the Pd activated surface.

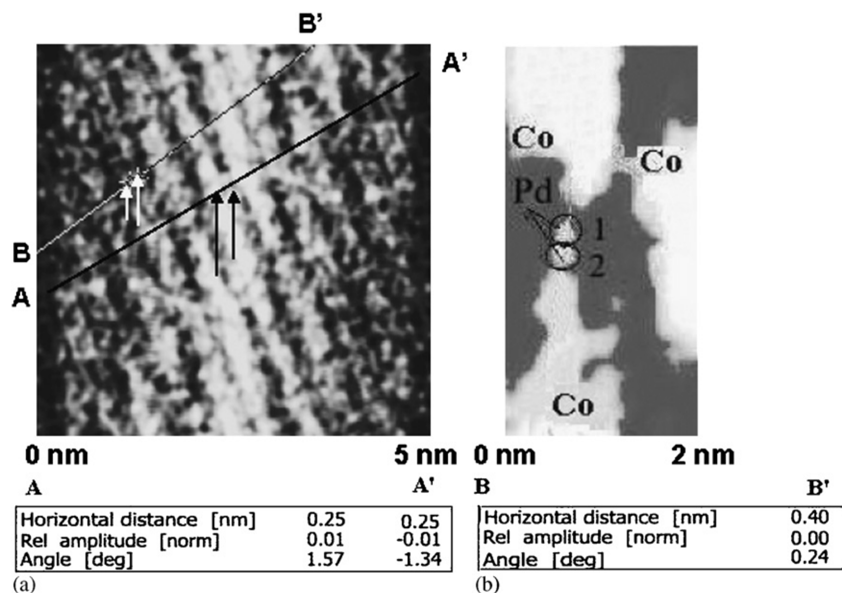

Horizontal distance [nm]	0.25	0.25
Rel amplitude [norm]	0.01	-0.01
Angle [deg]	1.57	-1.34

(a)

Horizontal distance [nm]	0.40
Rel amplitude [norm]	0.00
Angle [deg]	0.24

(b)

Fig. 5. STM images and profiles of Si surface after 1 s electroless deposition of Co(W,P) (a) in scanning scale of 5×5 nm. Two atomic spacings of 0.40 nm (A–A′ profile) and 0.25 nm (B–B′ profile) can be found respectively, (b) processed STM image of a 2×5 nm area of Pd clusters and Co(W,P) nuclei.

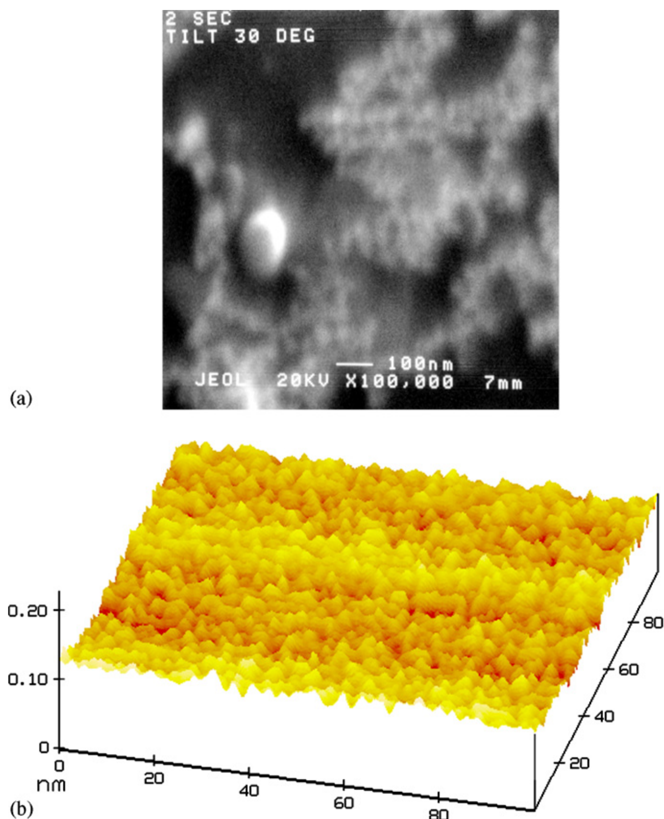

Fig. 6. Surface morphology of 2 s Co(W,P) nuclei: (a) SEM image, and (b) STM image in scanning size of 100 nm^2.

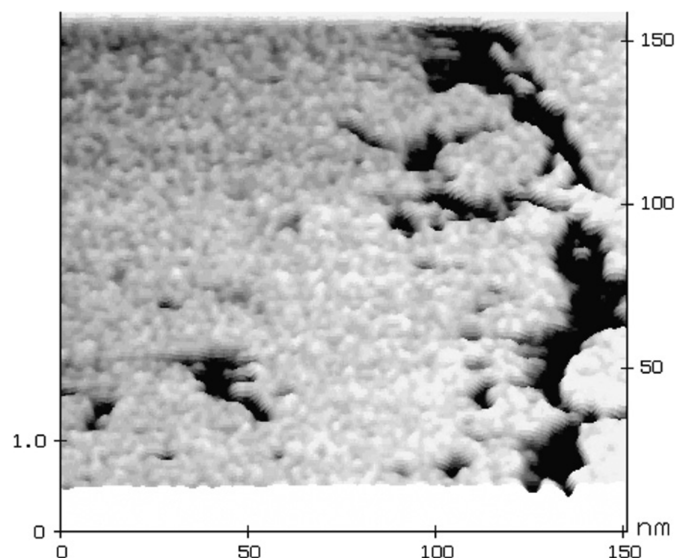

Fig. 7. Strong lateral coalescence of Co(W,P) nuclei after 3 s deposition.

This inhomogeneity is attributed to the wet chemically activated Si surface that is not fully and uniformly covered by Pd (refer to Fig. 1). The deposition does not initiate at every available site simultaneously on Si surface and this causes different rates of initial nucleation and film growth. Between 5 and 70 s, the mixed potential curve decreases from −0.37 to −0.70 V, and this indicates the full growth of Co layers may be associated with other deposition processes, probably involving the deposition of W and P species. The FI curve of Co(W,P) deposition gradually reaches a steady state (70 s$<t<$500 s). This flat slope of FI curve implies a slower deposition rate. This may be somewhat connected to the continuous nucleation mode, which is consistent with STM observations. The mixed potential is stabilized at −0.78 V and this implies that Co(W,P) is more easily deposited onto the Pd activated surface. From the viewpoint of electrochemistry, the

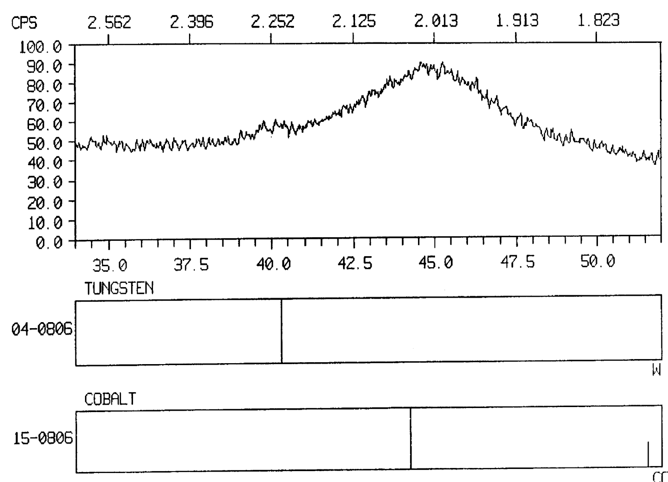

Fig. 8. Enhancement signal X-ray diffractogram of 10 s (CoW,P) deposit.

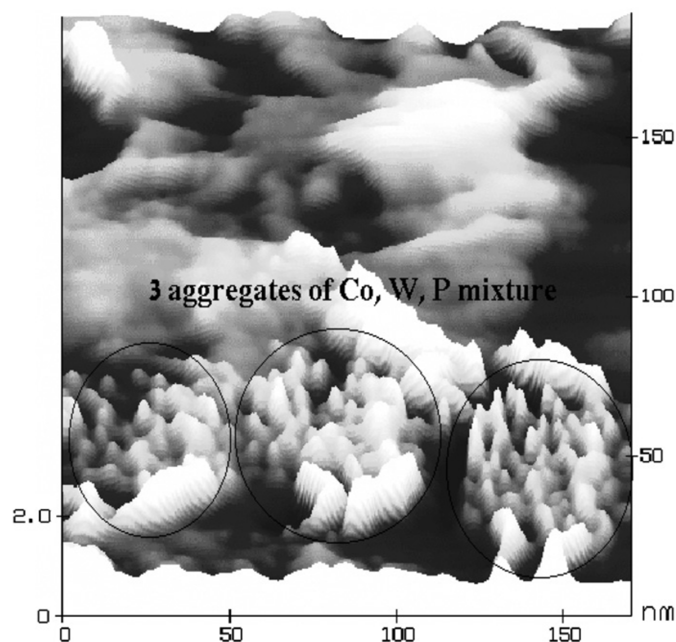

Fig. 9. Surface-view of Si surface after 10 s Co(W,P) deposition. New nodule nuclei, probably W and or P, start to emerge on the surface.

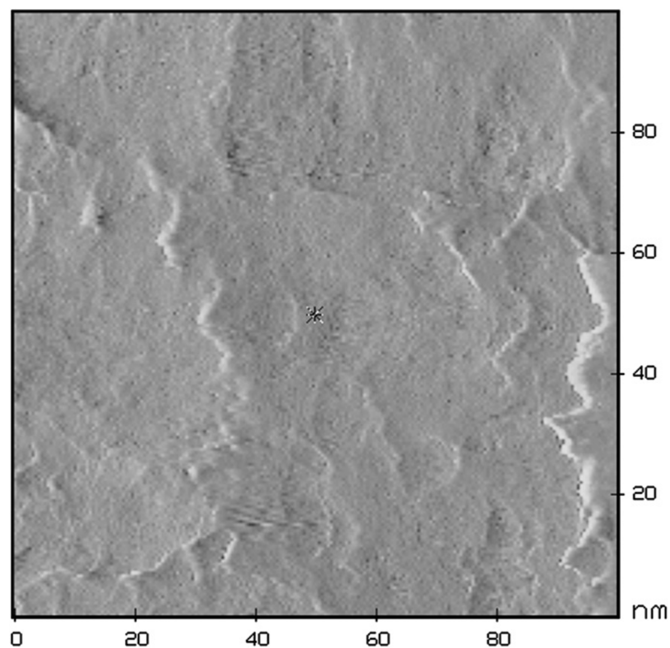

Fig. 10. Si surface after 45 s deposition of Co(W,P) showing continuous thin film layer by layer growth of Co(W,P), scanning scale is 100 × 100 nm.

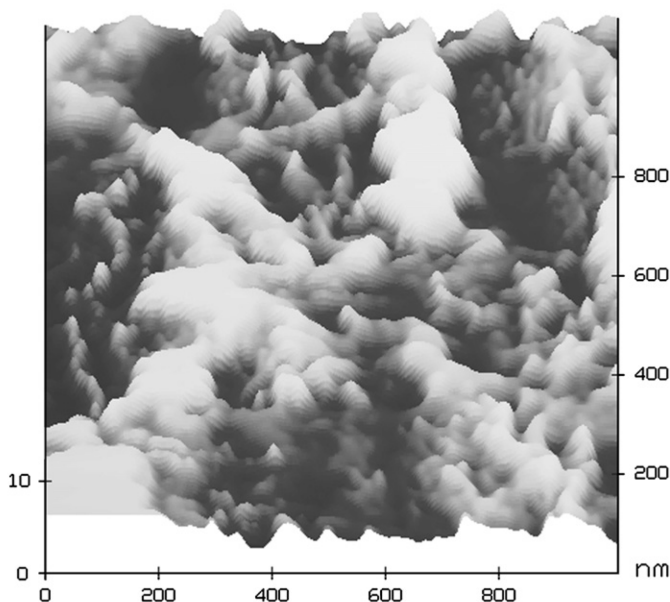

Fig. 11. Surface morphology of Si surface after prolonged deposition (10 min) of Co(W,P).

underlayer does not change the mixed potential of a reaction unless it is involved in the reaction. The relatively high negative value of mixed potential of Co(W,P) electroless deposition on Pd also reveals that Pd is actively involved in assisting Co deposition onto the Si substrate.

3.2.2. Morphology characterization and microstructure detection

Nakahara and Okinaka [18] reported that the seed layer determines the morphology of electroless deposit. Therefore, HRSEM and signal enhancement XRD were employed in this investigation to provide valuable information concerning the orientation and crystalline phase of Pd as well as its effect on the Co(W,P) thin film. High resolution SEM image of Co(W,P) deposited on Pd exhibits the obvious gap between the agglomerated grains and a fairly smooth feature (Fig. 13) and this is somewhat consistent of amorphous or multi-orientations of grain growth. The XRD pattern of a 2 min wet-deposition Pd underlayer sample (Fig. 14a) shows only one weak peak representing cubic Pd(111) at 40° around, along with a very pronounced (220) Si peak (56°, 2θ). The intensity of the unique Pd peak changes when the sample was rotated, revealing a domination of (111) texture of Pd deposits. A sharp peak located at 54.23° results from the Si

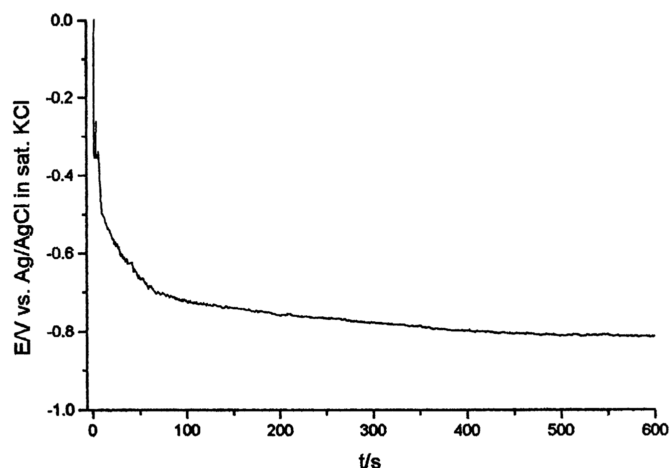

Fig. 12. Fast immersion curve of Co(W,P) deposited on Pd activated Si wafer surface.

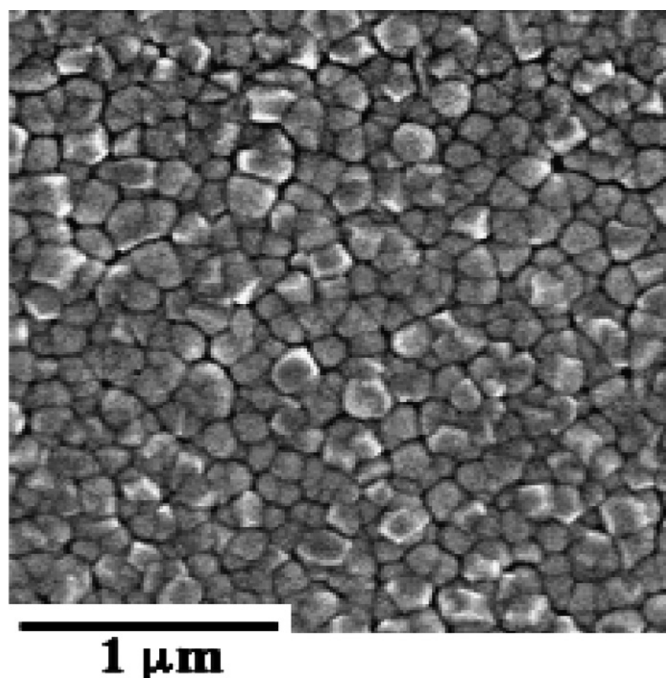

Fig. 13. High resolution SEM image of deposited Co(W,P) on Pd activated Si surface.

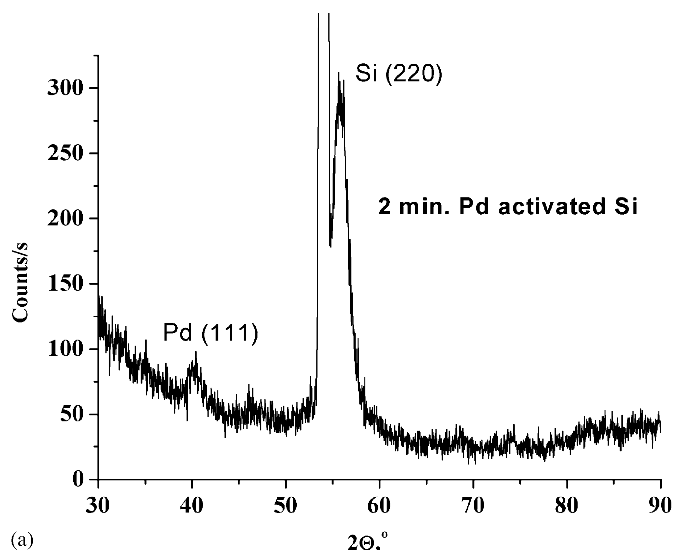

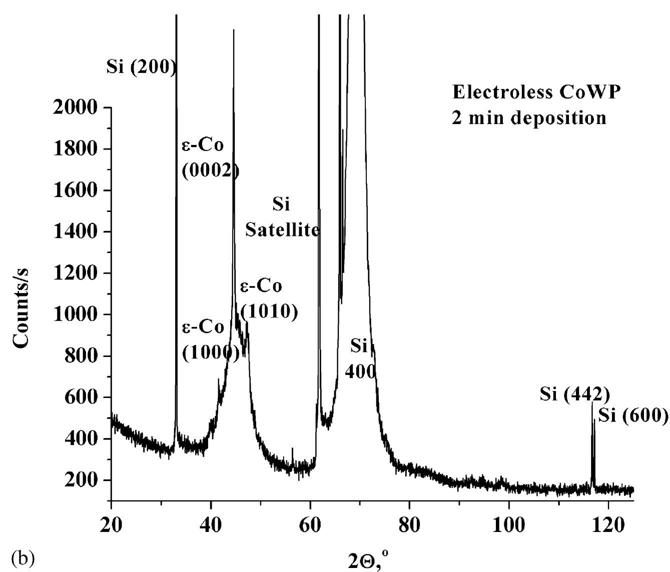

Fig. 14. (a) X-ray diffractogram of Si wafer surface after wet deposition of Pd for 2 min. (b) X-ray diffractogram of Co(W,P) electroless deposited on Pd activated Si surface for 2 min.

substrate. This peak can be attributed to Bremsstrahlung continuum radiation emitted from the X-ray source, which produces a diffracting deviation to the Si crystallographic planes. The X-ray diffractogram of 2 min electroless Co(W,P) on Pd activated Si surface (Fig. 14b) is assigned with three Miller indexes of Co crystalline planes (0002), (1010) and (1000). This signifies that the microstructure of the as-deposited film is the *hcp* phase of ε-Co with a different orientation and that is consistent with results from morphology characterization. The full width half maximum (FWHM) values of XRD peaks are of several degrees of nano-sized grains. The intensity ratio of the three X-ray peaks is: $I_{(0002)}:I_{(1010)}:I_{(1000)} = 7:2:1$. Thus, the strongest peak originating from (0002) is the result of the high degree of preferred orientation in the $\langle 0001 \rangle$ direction or *c*-axis perpendicular to the substrate.

3.3.3. Mean free path measured by XPS

Since Co has been tested as a barrier layer in semiconductor manufacturing [8], it is used here as a standard reference. The samples used in this XPS measurement have a metal-oxide-semiconductor (MOS) structure. The details of Co(W,P) MOS structure design were reported elsewhere [19,20]. The Co(W,P) deposition bath temperature during Co(W,P) electroless deposition was kept within the range of 90–91 °C [21,22] and the composition of Co(W,P) deposition bath is listed in Table 3. The inelastic mean free path of the diffused Cu

into Co(W,P) is introduced as a sensor to evaluate the barrier property of a novel material. The inelastic mean free path of electron of Co(W,P) layer was calculated using the following equation [23]:

$$\frac{I_{\mathrm{Co}}}{I_{\mathrm{Cu}}}(d) = \frac{I^0_{\mathrm{Co}}}{I^0_{\mathrm{Cu}}}[\exp(d/\lambda \sin\theta) - 1].$$

Here, d is the Co(W,P) thin layer thickness, θ is the angle between the sample surface and the XPS analyzer. For our measurements, $\theta = 90^\circ$ while I^0_{Co} and I^0_{Cu} are the XPS signal intensities from a clean Co and Cu substrates respectively. I_{Co} is the Co signal intensity from the thin Co(W,P) film. By using STM combined with alpha-step method, the deposited Co(W,P) layer is about 3 nm thick. I_{Cu} is the XPS signal intensity from the clean Cu substrate which is covered by the thin Co(W,P) layer. $I^0_{\mathrm{Co}}/I^0_{\mathrm{Cu}}$ and $I_{\mathrm{Co}}/I_{\mathrm{Cu}}$ are calculated to be 1.087 and 1.383 respectively. Consequently, λ was calculated to be 7.37 Å, which is significantly smaller than the inelastic mean free path value of 9.9 Å in the case of Cu diffused into Co [24]. This signifies that the Cu is more difficult to go through Co(W,P) without energy loss, and therefore Co(W,P) is a very effective barrier layer.

4. Discussion

4.1. The existence of W and P and their influence on the diffusion barrier quality

From XRD (Fig. 14), only Co peaks are observed. As measured by EDX, XPS and RBS (Rutherford backscattering spectroscopy, not shown here), the film contains about 2–4 at% and 8–10 at% of W and P, respectively. These concentrations are not beyond the detection limit of XRD instrument used in this work. XPS and TOF-SIMS (time-of-flight secondary ion mass spectroscopy) measurements also indicate that W can be found in the thin film. This implies that W is truly present in the sample despite the fact that there are no XRD peaks indicating the existence of P and W. Two tentative explanations of these observations could be as follows:

1. P and W are enriched at boundary.

It is well known that elements located at the grain boundary are difficult to detect by XRD. Moreover, Hono and Laughlin [25] provided the most direct proof of the "boundary effect". An EDX probe analysis conducted on a Co(P) sample showed that the center of individual large grains did not exhibit any evidence of P. Nevertheless, P was detected when the electron beam was focused on the triple point of grain boundaries. Our repeated SAM measurements with sputtering confirm that Co_2P can exist at or near boundary (not presented here) and this result is consistent with literature [26]. In addition, about 1.5 at% of W was found in the 400 nm thick Co(W,P) film via SIMS. All of this indicates that Co_2P and W could be present at the boundary and could play a major role in blocking the diffusion of Cu via the boundary.

2. P and W exist in the form of an amorphous phase.

This proposition could raise an argument since it is known that amorphous structure is expected to appear only when the P content in the thin films is more than 12 at% [27,28]. This P concentration has not been reached in electroless deposition of Co(W,P) (in our thin films, the maximum concentration of P is ca. 10 at%). Shacham-Diamand et al. have carefully studied the Co(W,P) crystal structure using both fine material and electronics methodologies [29] and reported that Co(W,P) matrix as-deposited can contain Co(W,P) amorphous structure and the *o*-Co_2P enriched grain boundaries. STM profiles measured on the small scales, 10×10 nm and 30×30 nm, also showed some typical amorphous regions in which the nano-sized grains were randomly distributed with obvious separation gap between each other. It can therefore be assumed that to a certain degree, W and P are amorphous. For W, TOF-SIMS and XPS confirmed that the oxygen concentration in the Co(W,P) film itself is about 1–2 at%. This excludes the possibility that W is present as an oxide inside the film. In addition, WO_3 and WO_2 at the surface of the top Co(W,P) layer could result from the oxidation of W [30]. The best known example is the oxidation of freshly prepared tungsten STM tip. When the fresh STM-tip is exposed to air for several hours, an amorphous layer consisting of oxidized tungsten (WO_3 and WO_2) can be detected [31]. It should be noted that the amorphous domain in the Co(W,P) film is expected, since it eliminates the short-circuit paths of the grain boundaries, improving the barrier properties.

5. Concluding remarks

The initial stage, comprising of nucleation and growth of electroless Co(W,P) deposition on Pd activited p-type Si(100), is studied by using STM, SAM, HRSEM and XRD. At the initial stages of deposition, Co(W,P) nucleates around the sites of Pd activating particles, followed by a strong lateral growth. Full coverage occurs after a short time (ca. 10 s), followed by a uniform vertical growth. Induced co-depositions of P and W take place in the period of vertical growth. The uniform thin Co(W,P) film can be obtained after 2 min of deposition. Prolonging the deposition time could cause high strain stress and defects in such films.

The mixed potential (MP) of Co(W,P) electroless deposited on Pd is -0.78 V versus Ag/AgCl as shown in the fast immersion curve and this indicated that it is easier to deposit Co(W,P) on Pd. XRD measurements show that the Pd seed layer has a domination of (111) texture and the microstructure of the as-deposited Co(W,P) film is mainly based on the *hcp* phase of ε-Co in several

degrees of nano-sized grains. The arrangement of Co(W,P) grains demonstrates the high degree of preferred orientation of the ⟨0001⟩ direction or c-axis perpendicular to the substrate.

The inelastic mean free path of diffused Cu in Co(W,P) thin films has been found to be 7.37 Å. This is significantly smaller than the value of 9.9 Å in pure Co, signifying that it is more difficult for Cu to go through Co(W,P) without energy loss. This feature makes Co(W,P) to be a very effective barrier layer.

Acknowledgments

The authors are grateful to Dr. K. Kjoller of Digital Instruments Co., USA, Dr. S. Cohn of Weizmann Institute of Science and Technology-Israeli Science Academy, Mrs. Elena Sverdlova of Tel-Aviv University of Israel, Dr. A. Kohn of University of Oxford, England, Dr. K.C. Wong of the University of British Columbia and Dr. M. Gattrell of National Research Council, Canada for their useful discussions and technical support.

References

[1] A.A. Istratov, E.R. Weber, Appl. Phys. A: Mater. Sci. Process. A 66 (1998) 123.
[2] J.S. Cho, H.K. Kang, S.S. Wong, Y. Shacham-Diamand, MRS Bul. XVIII 6 (1993) 31.
[3] Y. Shacham-Diamand, V. Dubin, M. Angyal, Thin Solid Films 262 (1995) 931.
[4] Y. Shacham-Diamand, V. Dubin, J. Microel. Eng. 33 (1997) 47.
[5] V.M. Dubin, Y. Shacham-Diamand, B. Zhao, P.K. Vasudev, J. Electrochem. Soc. 144 (1997) 898.
[6] T.B. Massalski, Binary Alloy Phase Diagrams, ASM International, Materials Park, OH, 1990, p. 2703.
[7] C.S. Shin, Y.W. Kim, D. Gall, J.E. Greene, I. Petrov, Thin Solid Films 402 (2002) 172.
[8] E.J. O'Sullivan, A.G. Schrott, M. Paunovic, C.J. Sambucetti, J.R. Marino, P.J. Bailey, S. Kaja, K.W. Semkow, IBM J. Res. Develop. 42 (1998) 607.
[9] M. Paunovic, P.J. Bailey, R.G. Schad, D.A. Smith, J. Electrochem. Soc. 142 (1994) 1843.
[10] S. Lopatin, Y. Shacham-Diamand, V. Dubin, J. Pellerin, B. Zhao, P.K. Vasudev, in: Proceedings of the Fall MRS Meeting, Boston, USA, December 2–5, 1996.
[11] S. Lopatin, Y. Shacham-Diamand, V. Dubin, P.K. Vasudev, in: Proceedings of 191st Meeting of the Electrochemical. Society, Montreal, Canada, May 28–31, 1997.
[12] S. Lopatin, Y. Shacham-Diamand, V. Dubin, P.K. Vasudev, in: Proceedings of 14th International VLSI Multilevel Interconnection Conference, Santa Clara, CA, USA, June 10–12, 1997.
[13] T. Homma, K. Naito, M. Takai, T. Osaka, Y. Yamazaki, T. Namikawa, J. Electrochem. Soc. 138 (1991) 1269.
[14] T. Homma, T. Yamazaki, T. Osaka, J. Electrochem. Soc. 139 (1992) 732.
[15] B.J. Hwang, S.H. Lin, J. Electrochem. Soc. 142 (1995) 3749.
[16] T. Homma, M. Tanabe, K. Itakura, T. Osaka, J. Electrochem. Soc. 144 (1997) 4123.
[17] (a) NanoScope II Manual, Digital Instruments Co., USA.;
(b) Private communication with Dr. K. Kjoller (Digital Instruments Co., USA) and Dr. S. Cohn (Weizmann Institute of Science and Technology-Israeli Science Academy).
[18] S. Nakahara, Y. Okinaka, Annul. Rev. Mater. Sci. 21 (1991) 93.
[19] A. Kohn, M. Eizenberg, Y. Shacham-Diamand, J. Appl. Phys. 92 (2002) 5508.
[20] A. Kohn, M. Eizenberg, Y. Shacham-Diamand, J. Appl. Phys. 94 (2003) 3015.
[21] Y. Shacham-Diamand, Y. Sverdlov, Microelectron. Eng. 50 (2000) 525.
[22] Y. Shacham-Diamand, S. Lopatin, Electrochim. Acta 44 (1999) 3639.
[23] D. Briggs, M.P. Seah, Practical Surface Analysis, second ed., Wiely, Chichester, 1990, pp. 151, 207–209, 490.
[24] U. Ramsperger, A. Vaterlaus, P. Pfäffli, U. Maier, D. Pescia, Phy. Rev. B. 53 (1996) 8001.
[25] K. Hono, D.E. Laughlin, J. Magn. Magn. Mater. 80 (1989) L137.
[26] A. Kohn, M. Eizenberg, Y. Shacham-Diamand, Y. Sverdlov, Mater. Sci. Eng. A 302 (2001) 18.
[27] K. Hüller, M. Sydow, G. Dietz, J. Magn. Magn. Mater. 53 (1985) 269.
[28] M.A. Sheleg, T.A. Tochitskii, L.V. Nemtsevich, Metallofizika 15 (1993) 77.
[29] A. Kohn, M. Eizenberg, Y. Shacham-Diamand, J. Appl. Phys. 94 (2003) 3810.
[30] M.S. Aouadi, R.R. Parsons, P.C. Wong, K.A.R. Mitchell, J. Vac. Sci. Technol. A 10 (1992) 273.
[31] A.D. Müller, F.M. Müller, M. Hietschold, F. Demming, J. Jersch, K. Dickmann, Rev. Sci. Instrum. 70 (1999) 3970.